A Simple and Efficient Method for Radial Distortion Estimation by Relative Orientation

Yansong Duan, Xiao Ling, Yongjun Zhang, Zuxun Zhang, Xinyi Liu, and Kun Hu

***Abstract*— In order to solve the accuracy problem caused by lens distortions of nonmetric digital cameras mounted on an unmanned aerial vehicle, the estimation for initial values of lens distortion must be studied. Based on the fact that radial lens distortions are the most significant of lens distortions, a simple and efficient method for radial lens distortion estimation is proposed in this paper. Starting from the coplanar equation, the geometric characteristics of the relative orientation equations are explored. This paper further proves that the radial lens distortion can be linearly estimated in a continuous relative orientation model. The proposed procedure only requires a sufficient number of point correspondences between two or more images obtained by the same camera; thus it is suitable for a natural scene where the lack of straight lines and calibration objects precludes most previous techniques. Both computer simulation and real data have been used to test the proposed method; the experimental results show that the proposed method is easy to use and flexible.**

***Index Terms*— Continuous relative orientation, linear estimation, radial lens distortion, relative flight height, vertical photography.**

I. Introduction

NOWADAYS, the nonmetric digital camera tends to replace the traditional photogrammetric camera in a variety of low-altitude photogrammetry system due to its economy and convenience. Since lens distortions of the nonmetric digital camera have a decisive effect on the accuracy of photogrammetric process, it is an essential work to calibrate the nonmetric digital camera. The pragmatic approach is to obtain the lens distortion parameters of the camera through calibration in laboratory before mounting it on an unmanned aerial vehicle (UAV). These parameters from calibration are then used in the photogrammetric process after imagery data collection. However, this approach may fail when strong shake happens, especially when an UAV takesoff or lands, which causes numerical variation in the lens distortion parameters of the camera. Moreover, in order to meet the needs of different application requirements, it is common to change the focal length (FL), even the camera lens. All these practical problems challenge the traditional approach and force us to seek a simple and efficient lens distortion estimation method.

Over the last 20 years, domestic and overseas scholars have carried out extensive research in camera calibration. Generally speaking, those works can be summarized into the following three categories.

1) *Calibration in Laboratory:* Tsai [1], and Hekkila and Silven [2] proposed simultaneous nonlinear optimization of camera orientation parameters and lens distortion parameters by observing a calibration object whose geometry in the 3-D space is known with very good precision. These techniques can achieve high geometrical accuracy, but require an expensive calibration apparatus and an elaborate setup.
2) *Calibration by Specific Scene Pattern:* Techniques in this category do not need any calibration object; instead they use the rigidity of the scene [3] or plumb lines [4]–[6] to provide constraints on the lens distortion parameters. However, these approaches are not applicable when the scene is in lack of straight lines and planar patterns. This is often the case for UAV imagery.
3) *Self-Calibration by Bundle Block Adjustment:* These techniques use neither calibration objects nor specific scene pattern, but only point correspondences between images [7]–[9]. Since the algebraic constraints on the lens distortion parameters provided by the correspondences are nonlinear, these techniques have high requirement on the quality of initial values of lens distortion parameters. As mentioned before, the initial values are usually not reliable for the cameras on UAV due to the significant shaking or device modification.

In conclusion, the first and second categories have specific requirements for site or scene pattern, and are not suitable for emergency situations, and the third one is unstable and its convergence is not guaranteed.

Our research is focused on a low-altitude photogrammetry system, particularly an unmanned aerial system (UAS), since the potential for using UASs is large. More and more nonmetric cameras are used in UASs to reduce costs, and UASs are gradually becoming accessible to the general public

Manuscript received March 30, 2017; revised May 15, 2017 and July 14, 2017; accepted July 29, 2017. Date of publication September 4, 2017; date of current version November 22, 2017. This work was supported in part by the National Natural Science Foundation of China under Grant 41571434, in part by the National Basic Geographic Information Project under Grant 2016KK0201, and in part by the Basic Surveying and Mapping Technology Project under Grant 2016KJ0201. *(Corresponding author: Xiao Ling.)*

Y. Duan, X. Ling, Y. Zhang, Z. Zhang, and X. Liu are with the School of Remote Sensing and Information Engineering, Wuhan University, Wuhan 430079, China (e-mail: ysduan@whu.edu.cn; zyl_whu@163.com; zhangyj@whu.edu.cn; zhangzx@cae.cn; liuxy0319@whu.edu.cn).

K. Hu is with the Key Laboratory of Technology in Geo-Spatial Information Processing and Application System, Institute of Electronics, Beijing 100190, China (e-mail: khu@mail.ie.ac.cn).

Color versions of one or more of the figures in this paper are available online at http://ieeexplore.ieee.org.

Digital Object Identifier 10.1109/TGRS.2017.2735188

0196-2892 © 2017 IEEE. Personal use is permitted, but republication/redistribution requires IEEE permission.
See http://www.ieee.org/publications_standards/publications/rights/index.html for more information.

who are not experts in photogrammetry. Therefore, flexibility, efficiency, and convenience are important. The radial lens distortion estimation method described in this paper was developed with these considerations in mind.

The proposed method only uses point correspondences from a few (at least two) images to estimate the radial lens distortion and the entire solution process is linear. There are two assumptions throughout this paper.

1) The distortion center is known. As pointed out in [10] and [11], the precise positioning of the distortion center does not strongly affect the correction, and has no effect on the geometry (i.e., relative orientation model) between a camera pair. Therefore, fixing the distortion center is a reasonable approximation.
2) At least a pair of images are acquired by the way of vertical photography (the banking angle is very small). A high level of redundancy (over 70% overlap) often occurs in an UAV mission [12]–[14], and nowadays, UAVs are equipped with global positioning systems (GPSs) and inertial measurement units (IMUs) [14], so it is easy to select a pair of stereo images satisfying the vertical photography condition.

It is important to point out that our goal in this paper is not to accurately estimate the lens distortion but to propose a method that provides a good initial estimation of radial lens distortion parameters. These initial values of lens distortion parameters can be further used as an input for bundle adjustment (BA) [7], [9] to obtain an accurate lens distortion.

Note that Fitzgibbon [11] developed a simultaneous linear estimation of multiple view geometry and lens distortion. His technique is more flexible than ours, but there are at most ten solutions that need to be checked, and only the radial lens distortion equation of two-view geometry was derived.

This paper is organized as follows. Section II includes three parts, which are a general radial lens distortion model, the basic theory about relative orientation, and a six-point algorithm, which is often applied to solve the variables of relative orientation. Section III describes the details about how to solve the radial lens distortion. Section IV provides the experimental results. Both the computer simulation and real data are used to validate the proposed method. Section V concludes the main contributions of this paper.

II. Background Knowledge

Our proposed method is based on the relative orientation, which is commonly used in photogrammetry to recover the relative geometry between multiple views (two or more). In this section, we introduce the radial lens distortion model, which we adopt, the coplanar equation of relative orientation, and a well-known six-point algorithm, which is often applied to solve the variables of relative orientation.

A. Radial Lens Distortion Model

A complete analytic model of lens distortions usually consists of radial lens distortions, tangential lens distortions, and decentering lens distortions. Out of these three types of distortions, radial lens distortion contributes the most in magnitude [1]. The radial distortion models use low-order polynomials [15], for example

$$\begin{aligned} x &= \check{x}(1+\kappa_1\check{r}^2+\kappa_2\check{r}^4) \\ y &= \check{y}(1+\kappa_1\check{r}^2+\kappa_2\check{r}^4) \\ \check{r}^2 &= \check{x}^2+\check{y}^2 \end{aligned} \tag{1}$$

where

- (x, y) ideal (distortion-free) image coordinates;
- $(\check{x}, \check{y})$ real (distorted) image coordinates;
- κ_1,κ_2 coefficients for radial lens distortion.

Note that throughout this paper, all points are expressed in a 2-D coordinate system with the origin at the distortion center.

Generally speaking, the term κ_1 alone will usually suffice in medium-accuracy applications of digital cameras to account for the commonly encountered third-order barrel distortion [3], [16]. In this respect, we can conclude (2) from (1) by omitting term κ_2

$$\begin{aligned} \delta x &= x-\check{x} = \check{x}\check{r}^2\kappa_1 \\ \delta y &= y-\check{y} = \check{y}\check{r}^2\kappa_1. \end{aligned} \tag{2}$$

The symbols $(\delta x, \delta y)$ are called the distortion corrections to (x, y).

B. Relative Orientation

The parameters for the transformation from the 3-D object world coordinate system to the camera 3-D coordinate system centered at the optical center are called the extrinsic parameters. There are six extrinsic parameters: three components for the location of optical center, and three Euler angles φ, ω, and κ that define a sequence of three elementary rotations around y-, x-, and z-axes, respectively. The angle φ is performed clockwise, while the others are anticlockwise.

Relative orientation can be defined as a method to compute the extrinsic parameters of the right image, given that the left image is fixed (the extrinsic parameters of the left image are known). To further simplify the computation, we usually assume that the position parameters and Euler angles of the left image are all zero, and thus the rotation matrix of left image is an identity matrix. Namely, the coordinate system for relative orientation is defined at the projective center of the left camera, XY plane is parallel to focal plane, and Z-axis is vertical to XY plane, pointing to the sky. As shown in Fig. 1, $B_x, B_y, B_z, \varphi', \omega'$, and κ' denote the extrinsic parameters of the right image, the pair $a \leftrightarrow a'$ denotes the correspondence, (u, v, w) denotes the vector $\vec{Sa}$, and (u', v', w') denotes the vector $\vec{S'a'}$. The coplanar equation (3) is established for a certain correspondence

$$F = \begin{vmatrix} B_x & B_y & B_z \\ u & v & w \\ u' & v' & w' \end{vmatrix} = 0 \tag{3}$$

where

$$\begin{bmatrix} u \\ v \\ w \end{bmatrix} = R_{\text{left}} \begin{bmatrix} x \\ y \\ -f \end{bmatrix}$$

$$\begin{bmatrix} u' \\ v' \\ w' \end{bmatrix} = R_{\text{right}} \begin{bmatrix} x' \\ y' \\ -f \end{bmatrix}$$

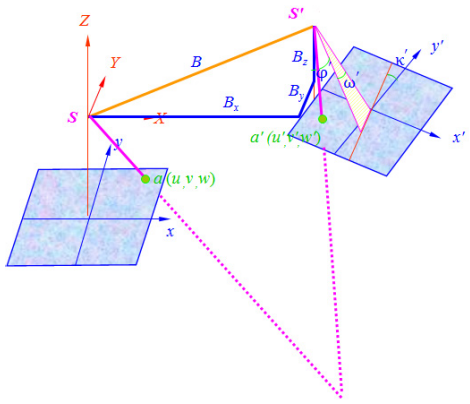

Fig. 1. Schematic of the relative orientation problem and the coplanar condition. S–XYZ is the 3-D coordinate system centered at the projective center of left image. S and S' are the projective centers of left and right camera, respectively. (x, y) and (x', y') are the 2-D coordinate systems of the ideal left and right images, respectively. B is the baseline between these two projective centers. The pair $a(u, v, w) \leftrightarrow a'(u', v', w')$ is the correspondence. $B_x, B_y, B_z, \varphi', \omega'$, and κ' denote the extrinsic parameters of the right image. Three vectors $\vec{B}$, $\vec{Sa}$, and $\vec{S'a'}$ are coplanar.

where

R_{left}	rotation matrix of the left image; here, it is the identity matrix;
R_{right}	rotation matrix of the right image, determined by $\varphi', \omega', \kappa'$;
(x, y)	ideal left image coordinates of the correspondence;
(x', y')	ideal right image coordinates of the correspondence;
f	FL of the camera.

Here, $B_y, B_z, \varphi', \omega'$, and κ' are the variables to be solved with respect to the scale factor B_x, so the coplanar equation is approximated by a Taylor expansion to the first order

$$F = F_0 + \frac{\partial F}{\partial B_y}\Delta B_y + \frac{\partial F}{\partial B_z}\Delta B_z + \frac{\partial F}{\partial \varphi'}\Delta\varphi' + \frac{\partial F}{\partial \omega'}\Delta\omega' + \frac{\partial F}{\partial \kappa'}\Delta\kappa' = 0. \quad (4)$$

Considering that $B_y, B_z, \varphi', \omega', and \kappa'$ are very small in vertical photography, the basic relationship formula among the variables of relative orientation can be further obtained after converting B_y and B_z to their corresponding values b_y and b_z in the image scale

$$V_q = \Delta b_y + \frac{y'}{f}\Delta b_z + \frac{x'y'}{f}\Delta\varphi' + \left(x + \frac{y'^2}{f}\right)\Delta\omega' + x'\Delta\kappa' - q$$
$$q \approx y - (y' + b_y). \quad (5)$$

The symbol q is known as vertical parallax. The derivation of coefficients in (5) can be found in [16].

C. Six-Point Algorithm

The six-point algorithm is widely adopted to solve the variables of relative orientation [16]. The spatial distribution of point correspondences on the overlap of two images is shown in Fig. 2.

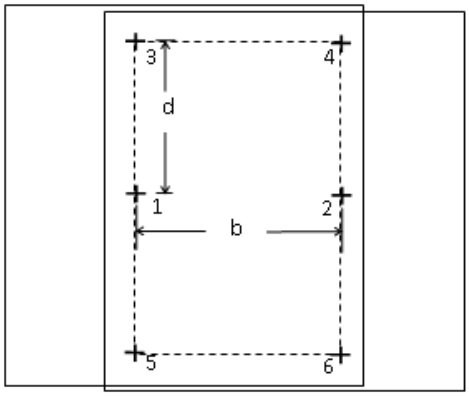

Fig. 2. Spatial distribution of point correspondences in the six-point algorithm. All six-point correspondences are numbered from 1 to 6, the distance between points 1 and 2 is denoted by symbol b, which is approximately equal to the baseline between two camera stations in the image scale, and the distance between points 1 and 3 is denoted by symbol d.

The spatial distribution of these six-point correspondences has the following properties [we denote the distortion corrections of the ith point in the jth image by $(\delta x_{ij}, \delta y_{ij})$, and its y-axis coordinate by y_{ij}; here $i = 1, 2, \ldots, 6$ is the point number and $j = 1, 2$ is the image number].

1) Point 1 is very close to the center of image 1, while point 2 is close to the center of image 2, so y_{11}, y_{12}, y_{21}, and y_{22} are approximately 0, and $\delta y_{11} = \delta y_{12} = \delta y_{21} = \delta y_{22} \approx 0$.
2) Points 3 and 5 are located symmetrically to point 1 and closed to the image boundaries, that is, $y_{31} = -y_{51}$ and $y_{32} = -y_{52}$; thus, $\delta y_{31} = -\delta y_{51}$ and $\delta y_{32} = -\delta y_{52}$. Points 4 and 6 share the similar relationship as points 3 and 5.

Each point correspondence can generate (5); there are six equations to solve five variables $b_y, b_z, \varphi', \omega'$, and κ'. The solution is listed here

$$b_y = \frac{1}{12d^2}\left[q_1\left(6f^2 + 4d^2\right) + q_2\left(6f^2 + 8d^2\right) - (q_3 + q_5)\left(3f^2 + 2d^2\right) - (q_4 + q_6)\left(3f^2 - 2d^2\right)\right]$$
$$b_z = \frac{f}{2d}(q_4 - q_6)$$
$$\varphi' = \frac{f}{2bd}(-q_3 + q_4 + q_5 - q_6)$$
$$\omega' = \frac{f}{4d^2}(-2q_1 - 2q_2 + q_3 + q_4 + q_5 + q_6)$$
$$\kappa' = \frac{1}{3b}[-q_1 + q_2 - q_3 + q_4 - q_5 + q_6] \quad (6)$$

where q_i is the vertical parallax of point i, which is defined by (5), and the symbols b and d are defined in Fig. 2.

III. Linear Estimation of Radial Lens Distortion

This section provides the details on how to effectively solve the radial lens distortion. We start with the linear solution from the two-view geometry, then show the geometric interpretation of it, and expand it to N-view geometry.

A. Linear Estimation of κ_1 From Relative Orientation Model

As mentioned in Section I, we assume that all input images are acquired by the way of vertical photography, so every

term of (6) is expected to be close to zero after the relative orientation process has been completed. However, that is not true if there exists radial lens distortion. The term q_i is appreciably influenced by radial lens distortion, and the relationship between these two quantities is expressed as follows:

$$\begin{aligned} q_i &\approx \check{y}_{i1} - (\check{y}_{i2} + b_y) \\ &= (y_{i1} - \delta y_{i1}) - (y_{i2} - \delta y_{i2} + b_y) \\ &= [y_{i1} - (y_{i2} + b_y)] - (\delta y_{i1} - \delta y_{i2}) \\ &= -\delta y_{i1} + \delta y_{i2} \end{aligned} \tag{7}$$

where y_{i1} and y_{i2} are the ideal y-axis coordinates of point i, which obeys the coplanar equation, that is, $y_{i1} - (y_{i2} + b_y) = 0$.

We can further obtain the following array when applying the properties of the six-point algorithm:

$$\begin{aligned} q_1 &= q_2 = 0 \\ q_3 &= -q_5 = -\delta y_{31} + \delta y_{32} \\ &= -d(d^2)\kappa_1 + d(d^2 + b^2)\kappa_1 = db^2\kappa_1 \\ q_4 &= -q_6 = -\delta y_{41} + \delta y_{42} \\ &= -d(d^2 + b^2)\kappa_1 + d(d^2)\kappa_1 = -db^2\kappa_1. \end{aligned} \tag{8}$$

Equation 6 is simplified to (9) after these constraints as described earlier are plugged into it

$$\begin{aligned} b_y &= 0 \\ b_z &= \frac{f}{d} q_4 = -fb^2\kappa_1 \\ \varphi' &= \frac{f}{bd}(-q_3 + q_4) = -2fb\kappa_1 \\ \omega' &= 0 \\ \kappa' &= 0. \end{aligned} \tag{9}$$

Equation 9 shows that the terms b_z and φ' are more significantly affected by the radial lens distortion than other terms. From this observation stems the idea to use b_z or φ' to estimate κ_1. That is, after the relative orientation process has been completed, the radial lens distortion κ_1 can be calculated from

$$\kappa_1 = -\frac{\varphi'}{2fb}$$

and

$$\kappa_1 = -\frac{b_z}{fb^2}. \tag{10}$$

B. Geometric Interpretation

Equation 9 shows that, if κ_1 is positive, the term b_z will be negative, that is, the flight strip will bend downward; otherwise, it will bend upward after the initial relative orientation process has been completed. The relationship between b_z and φ' can be comprehended from Fig. 3.

The details marked in blue circle in Fig. 3 show that

$$\begin{aligned} b_z &= b/2 \times \sin(\varphi') \approx b/2 \times \varphi' \\ &= b/2 \times -2fb\kappa_1 = -fb^2\kappa_1 \end{aligned}$$

thus (9), $b_z = -fb^2\kappa_1$, and $\varphi' = -2fb\kappa_1$ provide a self-consistent description (when A is small, $\sin A \approx A$).

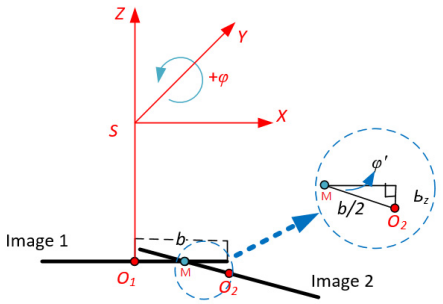

Fig. 3. Illustration of the influence of positive κ_1 on the terms b_z and φ' after the initial relative orientation process has been completed. S–XYZ is the 3-D coordinate system centered at the projective center of the first image. O_1 and O_2 are two image centers, respectively. The symbol b represents the distance between these two image centers in the image scale as before. Point M is the middle point between two image centers. Blue circle: geometric relation between b_z and φ'.

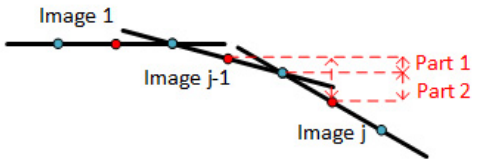

Fig. 4. Illustration of b_{zj} and φ_j between image $j-1$ and image j ($j = 2, 3, \ldots, n$). Red dots: image centers. Blue dots: middle point between adjacent images. The term φ_j is a constant value, which is just the same as the value φ_2 between images 1 and 2, while the term b_{zj} is complex and made up of two parts.

C. Linear Estimation of κ_1 From Continuous Relative Orientation Model

In practical applications, we should adopt multiple continuous images, all adjacent images of which have similar overlap ratio, to enhance the reliability of estimation.

Assuming the total number of images is n, the camera 3-D coordinate system of image 1 is taken as a reference coordinate system, the symbols b_{zj} and φ_j denote the relative flight height and relative banking angle between images $j-1$ and j, and the symbols $(b_z)_j$ and $(\varphi)_j$ denote the relative flight height and relative banking angle between images 1 and j. After continuous relative orientation process has been completed, as shown in Fig. 4, $(b_z)_n$ and $(\varphi)_n$ can be computed as follows.

1) From (9)

$$\begin{aligned} (b_z)_1 &= 0 \quad (b_z)_2 = -fb^2\kappa_1 \\ (\varphi)_1 &= 0 \quad (\varphi)_2 = -2fb\kappa_1. \end{aligned}$$

2) φ_j is a constant value for all $j = 2, 3, \ldots, n$, and thus

$$(\varphi)_n = (n-1) \times (\varphi)_2 = -2(n-1)fb\kappa_1.$$

3) b_{zj} can be computed from two parts (Fig. 4):

a) Part 1

$$\begin{aligned} &\frac{(b_z)_2}{\sin[(\varphi)_2]} \times \sin[(\varphi)_{j-1}] \\ &\quad = (b_z)_2 \times \frac{\sin[(j-2) \times (\varphi)_2]}{\sin[(\varphi)_2]} \approx (j-2)(b_z)_2. \end{aligned}$$

b) Part 2

$$\frac{(b_z)_2}{\sin[(\varphi)_2]} \times \sin[(\varphi)_j] \approx (j-1)(b_z)_2.$$

Thus

$$b_{zj} = (j-2)(b_z)_2 + (j-1)(b_z)_2 = (2j-3)(b_z)_2.$$

Finally

$$\begin{aligned}(b_z)_n &= \sum_{j=2}^{n} b_{zj} \\ &= \sum_{j=2}^{n} (2j-3)(b_z)_2 \\ &= (b_z)_2 + (2*3-3)(b_z)_2 + \cdots + (2n-3)(b_z)_2 \\ &= (n-1)^2 (b_z)_2 \\ &= -(n-1)^2 f b^2 \kappa_1.\end{aligned}$$

In summary, the term κ_1 can be calculated from the continuous relative orientation model as

$$\kappa_1 = -\frac{(\varphi)_n}{2(n-1)fb}$$

and

$$\kappa_1 = -\frac{(b_z)_n}{(n-1)^2 f b^2}. \tag{11}$$

There are two conclusions from (11).

1) If there exists radial lens distortion, the relative angle φ will increase or decrease with an image number n linearly, while the relative height b_z will act like a part of a parabola.
2) Although κ_1 can be obtained from both $(\varphi)_n$ and $(b_z)_n$, there is a difference in the stability of those results. Since the formula from $(\varphi)_n$ is simpler than the formula from $(b_z)_n$, the result from $(\varphi)_n$ will have smaller standard deviation.

We will return back to this point later.

D. Summary

The recommended estimation procedure is as follows.

1) Choose a few (at least two) continuous images, which satisfy a vertical photographic condition and have a similar overlap ratio. It is not a hard work for UAV images with the help of GPSs and IMUs data.
2) Obtain at least six standard point correspondences between each pair of consecutive images by auto-matching or manual selection.
3) Use the six-point algorithm to compute the parameters of relative orientation.
4) Estimate the term κ_1 by (11). Here, estimating by the relative banking angle φ is recommended.
5) Apply radial distortion correction with κ_1 to each point in every image according to (2).

If an accurate camera information is required, BA, initialized with reasonable estimation of κ_1 using the method proposed in this paper, should be applied to achieve the final result.

IV. Experiments

The proposed method has been tested on both computer simulated data and real data. The experimental procedures and results will be discussed in detail in this section.

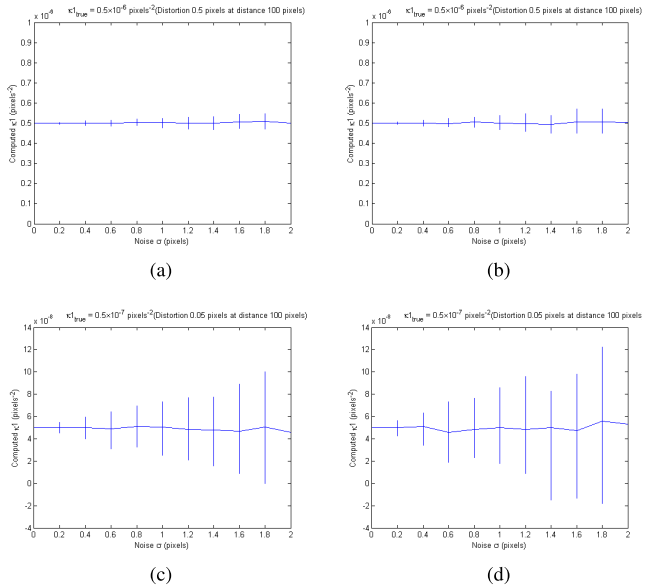

Fig. 5. Tests on computer simulated data. Simulated image size is 640×480. The graphs show the computed radial lens distortion κ_1 as a function of noise level on the 2-D points. (a) and (c) Results obtained from φ'. (b) and (d) Results obtained from b_z. Standard deviations increase with the increase of noise, and are more pronounced on images with less distortion. The results from φ' have smaller standard deviations than those from b_z as expected.

A. Tests on Computer Simulated Data

In order to gain a feeling for the performance of the distortion estimation algorithm with two views under typical image noise conditions, an investigation with simulated data was conducted. A realistic scene was generated using two camera positions, both of which have over 60% overlap and satisfy the vertical photographic condition, and six 3-D points. These points and cameras were used to generate perfect 2-D points close to the six standard positions, and then Gaussian noise was added to record the behavior of the estimate κ_1. The testing procedure was as follows.

1) Given six 3-D points $\{X_i\}_{i=1}^{6}$ and two camera positions, generate point correspondences close to the six standard positions. Distort the perfect correspondences to generate noiseless correspondences $\bar{x}_i \leftrightarrow \bar{x}_i'$.
2) Repeat 100 times.
   a) Draw noise from a Gaussian distribution of standard deviation σ, and add to $\bar{x}_i \leftrightarrow \bar{x}_i'$ to generate noisy correspondences $x_i \leftrightarrow x_i'$.
   b) Use (6) to recover the relative orientation model, mainly the terms φ' and b_z.
   c) Use (10) to compute two results of κ_1 from φ' and b_z, respectively.
3) From the list of computed κ_1 values, compute the median and the 10th and 90th percentile points. These are shown in Fig. 5.

The noise levels used had σ between 0 and 2 pixels, which represents a typical range in video and film imagery [11].

There are some conclusions about the proposed method from Fig. 5. For the distortion of about 20 pixels at the image corner, the estimation results have good accuracy (within 10% of the veridical value) even when the noise level is two pixels.

TABLE I
ORIGINAL CONTINUOUS RELATIVE ORIENTATION RESULT. FL: FOCAL LENGTH

Image No.	b_x(FL)	b_y(FL)	b_z(FL)	φ(rad)	ω(rad)	κ(rad)
1003	0	0	0	0	0	0
1004	100.000	-11.974	-0.597	-0.0159636	0.0153319	0.014935
1005	199.355	-27.854	-0.739	-0.0263082	0.0218664	0.038450
1006	294.691	-47.801	-1.727	-0.0428865	0.0225442	0.030821
1007	399.373	-74.418	-5.973	-0.0543432	0.0147505	0.024925
1008	508.638	-81.899	-9.307	-0.0637817	0.0357364	-0.004675
1009	613.867	-109.079	-14.963	-0.0785231	0.0282453	-0.007054
1010	713.365	-135.446	-19.759	-0.0851849	0.0189008	0.013577
1011	808.674	-155.008	-25.972	-0.0989651	0.0208383	-0.050076

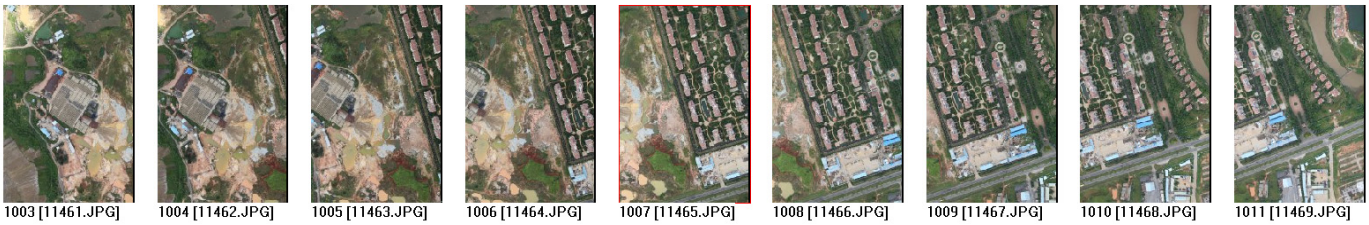

Fig. 6. Nine continuous images for experiment. The flight height range is from 819 to 822 m, the overlap between adjacent images is about 75%, and the covered land is an urban fringe.

TABLE II
ESTIMATION RESULTS OF κ_1 ACCORDING TO OUR PROPOSED METHOD

Image Number Range	$(b_z)_n$(FL)	$(\varphi)_n$(rad)	κ_1 Estimated by $(b_z)_n$	κ_1 Estimated by $(\varphi)_n$
1003∼1004	-0.597	-0.0159636	5.9700×10^{-5}	7.9818×10^{-5}
1003∼1005	-0.739	-0.0263082	1.8475×10^{-5}	6.5771×10^{-5}
1003∼1006	-1.727	-0.0428865	1.9189×10^{-5}	7.1478×10^{-5}
1003∼1007	-5.973	-0.0543432	3.7331×10^{-5}	6.7929×10^{-5}
1003∼1008	-9.307	-0.0637817	3.7228×10^{-5}	6.3782×10^{-5}
1003∼1009	-14.963	-0.0785231	4.1564×10^{-5}	6.5436×10^{-5}
1003∼1010	-19.759	-0.0851849	4.0325×10^{-5}	6.0846×10^{-5}
1003∼1011	-25.972	-0.0989651	4.0581×10^{-5}	6.1853×10^{-5}

But, if the distortion at the image corner is two pixels, which is in the same magnitude with noise, the estimation results will be unreliable. Thus, this technique cannot give reliable estimates of κ_1, when the amount of distortion is not one magnitude higher than the noise level. Moreover, the estimates computed from φ' have smaller standard deviation than those computed from b_z as expected in Section III-C, so it is better to use φ' to compute κ_1.

B. Tests on Real Data

Multiple images from an UAV mission are further used to evaluate the performance of the proposed method on the real data. The nonmetric camera is Cannon EOS 5D Mark II, whose image size is 5616 pixel × 3744 pixel, pixel size is 6.41 μm, and FL is 24.5724 mm. Nine continuous images from a strip are selected according to their Positioning and Orientation System data: the flight height range is from 819 to 822 m, the overlap between adjacent images is about 75%, and the covered land is an urban fringe, as shown in Fig. 6.

To obtain some correspondences (at least six) from each image with its next image, this paper employed an auto image match method to achieve a certain amount of correspondences, then checked the match result to exclude the outliers by manual inspection, and at last there remained totally 95 reliable correspondences, the distribution of which are shown in Fig. 7, with a localization accuracy of better than 0.3 pixels.

All the 95 correspondences have been used to process the continuous relative orientation, and the scale factor b_x between the first-image center and the second-image center is set to be 100 FL to simplify the calculation, that is, $b \approx 100$ FL. The results are shown in Table I, and Fig. 8 shows the trend of the relative flight height b_z and relative angle φ.

The records of Table I and the trend charts in Fig. 8 show the relative angle decreases linearly and the flight strip significantly bends downward close to a part of parabola; both these phenomena indicate that radial distortion exists in the camera. Thus, our proposed method was applied to estimate the distortion κ_1. The estimation results from only two images to all nine images are listed in Table II.

Table II shows that all estimation results of κ_1 obtained by either $(b_z)_n$ or $(\varphi)_n$ are in the same magnitude and tend to be stable. The radial lens distortion was then removed for all point correspondences in all images using the value of $\kappa_1 = 6.1853 \times 10^{-5}$ computed from $(\varphi)_9$ and (2). Continuous relative orientation was carried out based on the distortion-free

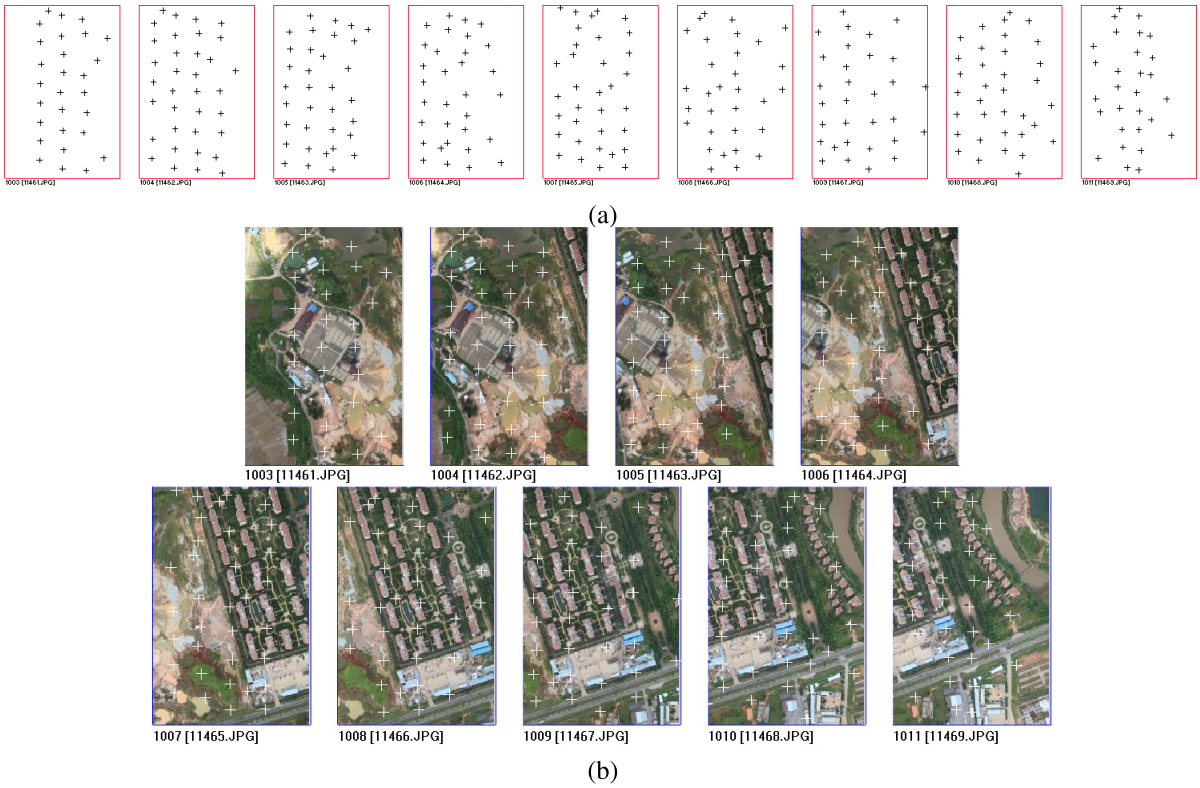

Fig. 7. Distribution of correspondences in continuous images. (a) Distribution diagram of correspondences. Red rectangles: nine images. Black crosses: correspondences, and it shows that all six standard position are covered. (b) Correspondences in nine images. White crosses: correspondences.

TABLE III

RESULTS FOR CONTINUOUS RELATIVE ORIENTATION USING DISTORTION PARAMETERS COMPUTED BY THE PROPOSED METHOD

Image No.	b_x(FL)	b_y(FL)	b_z(FL)	φ(rad)	ω(rad)	κ(rad)
1003	0	0	0	0	0	0
1004	100.000	-12.720	1.332	-0.00667	0.015590	0.014424
1005	198.979	-28.955	2.679	-0.00713	0.021205	0.037577
1006	294.547	-48.887	2.597	-0.01539	0.019811	0.029571
1007	399.181	-74.928	1.822	-0.01711	0.008181	0.023446
1008	507.971	-83.297	2.303	-0.01549	0.029929	-0.006460
1009	613.276	-110.389	0.464	-0.02043	0.019359	-0.009260
1010	710.900	-136.111	-0.309	-0.01410	0.005914	0.011122
1011	806.491	-155.624	-2.629	-0.03108	0.005611	-0.052900

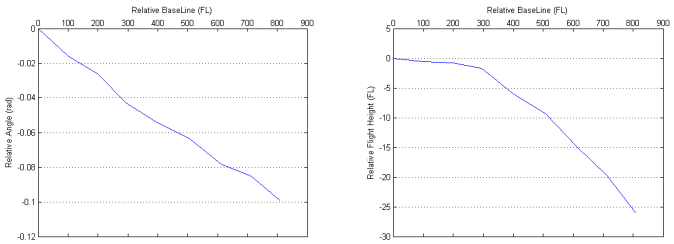

Fig. 8. Trend charts of relative angle φ and relative flight height b_z, both of which indicate there exists the radial lens distortion. (a) Trend chart of relative angle, the shape of which is approximately a straight line. (b) Trend chart of flight height, the shape of which is approximately a part of parabola.

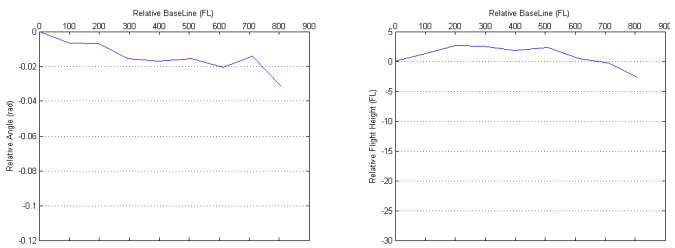

Fig. 9. Variations of relative angle and relative flight height after the radial distortion has been removed by the proposed method. (a) There is no obvious tendency found in relative angle. (b) There is no obvious tendency found in relative flight height.

point correspondences. Table III shows the result of this continuous relative orientation, and Fig. 9 shows both the trend of corrected relative flight height and the relative angle.

The comparison of Figs. 8 and 9 shows that the distortion correction effectively eliminates the obvious tendencies of relative angle and relative flight height, which may affect the

TABLE IV
CONTINUOUS RELATIVE ORIENTATION RESULT FROM STRICT CALIBRATION COMPARED WITH THE PROPOSED METHOD

Image No.	b_x(FL)	b_y(FL)	b_z(FL)	φ(rad)	ω(rad)	κ(rad)	The difference of b_z between two method	The difference of φ between two method
1003	0	0	0	0	0	0	0	0
1004	100.000	-12.999	1.728	-0.00233	0.015634	0.015434	0.396	0.00434
1005	202.153	-29.551	2.984	-0.00406	0.021234	0.038559	0.305	0.00307
1006	301.402	-49.168	2.953	-0.01447	0.018428	0.030409	0.356	0.00092
1007	408.850	-74.913	2.156	-0.01622	0.005027	0.023700	0.334	0.00089
1008	519.045	-83.497	2.786	-0.01178	0.026997	-0.005450	0.483	0.00371
1009	627.404	-110.517	1.156	-0.01678	0.015043	-0.008140	0.692	0.00365
1010	727.374	-136.239	0.686	-0.00941	0.000439	0.012343	0.995	0.00469
1011	825.611	-156.067	-1.928	-0.02787	-0.000310	-0.052050	0.701	0.00321

convergence property and convergence efficiency of subsequent processing (e.g., BA).

The nonmetric camera was calibrated in a professional institution to get the accurate values of the lens distortion parameters for further comparative analysis. The calibration result shows $\kappa_1 = 5.5475 \times 10^{-5}$ and $\kappa_2 = -2.80\,963 \times 10^{-8}$, which indicates that the two values of κ_1 are in the same magnitude and quite close. A continuous relative orientation was then implemented from point correspondences corrected for radial distortion via κ_1 and κ_2 values determined from laboratory calibration. These two results for the continuous relative orientation parameters from our method and the laboratory calibration are displayed in Table IV.

Table IV shows that the differences in relative flight height and relative angle between these two results are not pronounced, and in practice, these differences can easily be compensated in self-calibration BA by applying the estimation of κ_1 as an initial value. Therefore, the experimental results show that our method can estimate the radial lens distortion κ_1 with a high precision and improve the accuracy of the continuous relative orientation.

V. CONCLUSION

In this paper, we have developed a simple and efficient method for estimating the radial lens distortion coefficient. The method uses a few-point correspondences from at least two images, which satisfy the vertical photographic condition, to recover the relative orientation model, and then employs a linear algorithm to estimate the radial distortion. Since: 1) there are no specific requirements for site or scene pattern (e.g., plumb lines); 2) the estimation algorithm is linear and has a good precision; and 3) selecting a few images acquired by the way of vertical photography is easy for UAV, the proposed method is suitable for UAV to estimate its radial lens distortion, especially during an emergency.

This paper has two main contributions:

1) *Detection of the Radial Lens Distortion:* The mathematical relationships between the radial lens distortion and relative flight height and relative angle were deduced. If there exists radial lens distortion, the relative angle will increase or decrease with image number linearly, while the relative height will act as a parabola, after relative orientation process completes. These interesting relationships can be used in turn to detect whether there exists radial lens distortion. That is, we first process the continuous relative orientation among a few (better more than six) images, then draw the trend charts of relative angle and relative flight height with the image number (or relative baseline) as variable, and finally check whether the relative angle has an obvious linear change (increase or decrease) and the trend curve of relative flight height is close to a part of a parabola. If both the trends are observed, there exists a significant radial distortion in the camera.
2) *Linear Estimation of the Radial Lens Distortion:* The radial lens distortion detected on the camera can be linearly estimated by our method. All the experimental results show that the estimates by our method have good accuracy (within 20% of the veridical value). These estimates can be further applied to improve the accuracy of the continuous relative orientation, even the convergence property, and the convergence efficiency of BA.

Although the proposed method cannot meet the requirement of high accuracy, it is quite effective and simple as a kind of method to estimate the initial value of the radial distortion. Therefore, the proposed method is very helpful for UAS if the camera has not been strictly calibrated.

REFERENCES

[1] R. Y. Tsai, "A versatile camera calibration technique for high-accuracy 3D machine vision metrology using off-the-shelf TV cameras and lenses," *IEEE J. Robot. Autom.*, vol. 3, no. 4, pp. 323–344, Aug. 1987.
[2] J. Heikkila and O. Silvén, "A four-step camera calibration procedure with implicit image correction," in *Proc. IEEE Comput. Soc. Conf. Comput. Vis. Pattern Recognit.*, Jun. 1997, pp. 1106–1112.
[3] Z. Zhang, "A flexible new technique for camera calibration," Microsoft Res., Redmond, WA, USA, Tech. Rep. MSR-TR-98–71, Dec. 1998.
[4] D. C. Brown, "Decentering distortion of lenses," *Photogramm. Eng.*, vol. 32, no. 3, pp. 444–462, 1966.
[5] F. Devernay and O. D. Faugeras, "Automatic calibration and removal of distortion from scenes of structured environments," in *Proc. Int. Symp. Opt. Sci., Eng., Instrum. Int. Soc. Opt. Photon.*, Jul. 1995, pp. 62–72.
[6] S. B. Kang, "Semiautomatic methods for recovering radial distortion parameters from a single image," Cambridge Res. Lab., Cambridge, MA, USA, Tech. Rep. CRL 97/3, May 1997.
[7] O. D. Faugeras, Q.-T. Luong, and S. J. Maybank, "Camera self-calibration: Theory and experiments," in *Proc. 2nd Eur. Conf. Comput. Vis.*, May 1992, pp. 321–334.
[8] Y. Zhang, "Camera calibration using 2D-DLT and bundle adjustment with planar scenes," *Editoral Board Geomatics Inf. Sci. Wuhan Univ.*, vol. 27, no. 6, pp. 566–571, 2002.
[9] Q. T. Luong and O. D. Faugeras, "Self-calibration of a moving camera from point correspondences and fundamental matrices," *Int. J. Comput. Vis.*, vol. 22, no. 3, pp. 261–289, 1997.

[10] R. C. Willson and S. A. Shafer, "What is the center of the image?" in *Proc. IEEE Conf. Comput. Vis. Pattern Recognit.*, Jun. 1993, pp. 670–671.
[11] A. W. Fitzgibbon, "Simultaneous linear estimation of multiple view geometry and lens distortion," in *Proc. IEEE Conf. Comput. Vis. Pattern Recognit.*, Dec. 2001, pp. 125–132.
[12] H. Eisenbeiss and M. Sauerbier, "Investigation of UAV systems and flight modes for photogrammetric applications," *Photogramm. Rec.*, vol. 26, no. 136, pp. 400–421, 2015.
[13] N. Haala, M. Cramer, F. Weimer, and M. Trittler, "Performance test on UAV-based photogrammetric data collection," *Int. Arch. Photogramm., Remote Sens. Spatial Inf. Sci.*, vol. 38-1/C22, no. 1, pp. 7–12, 2012.
[14] D. Turner, A. Lucieer, and L. Wallace, "Direct georeferencing of ultrahigh-resolution UAV imagery," *IEEE Trans. Geosci. Remote Sens.*, vol. 52, no. 5, pp. 2738–2745, May 2014.
[15] R. Szeliski, *Computer Vision: Algorithms and Applications*. London, U.K.: Springer, 2010.
[16] C. C. Slama, Ed., *Manual of Photogrammetry*, 4th ed. Lake Elmo, MN, USA: American Society of Photogrammetry, 1980.

Yansong Duan was born in 1975. He received the M.S. and Ph.D. degrees from Wuhan University, Wuhan, China, in 2009 and 2016, respectively.

He is currently a Teacher with the School of Remote Sensing and Information Engineering, Wuhan University. His research interests include photogrammetry; image matching, 3-D city reconstruction, and high-performance computing with GPU.

Xiao Ling was born in 1989. He received the B.S. and M.S. degrees from Wuhan University, Wuhan, China, in 2012 and 2014, respectively, where he is currently pursuing the Ph.D. degree.

His research interests include photogrammetry, computer vision, camera calibration, and image matching.

Yongjun Zhang was born in 1975. He received the B.S., M.S., and Ph.D. degrees from Wuhan University, Wuhan, China, in 1997, 2000, and 2002, respectively.

He is currently a Professor of photogrammetry and remote sensing with the School of Remote Sensing and Information Engineering, Wuhan University. His research interests include space, aerial, and low-altitude photogrammetry, image matching, combined bundle adjustment with multisource data sets, 3-D city reconstruction, and industrial inspection.

Zuxun Zhang is an expert in photogrammetry and remote sensing. He invented VirtuoZo, a digital photogrammetric system which has been promoted widely in China and abroad. In recent years, he has been devoted to the application of digital photogrammetric system in engineering design, engineering surveying, and digital city construction.

Prof. Zhang became a member of the International Academy of Sciences for Europe and Asia in 1995 and a member of the Chinese Academy of Engineering in 2003.

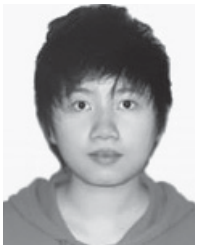

Xinyi Liu received the B.S. degree in engineering from Wuhan University, Wuhan, China, in 2014, where she is currently pursuing the Ph.D. degree with the School of Remote Sensing and Information Engineering.

Her research interests include 3-D reconstruction, texture mapping, and computational origami.

Kun Hu was born in 1986. He received the B.S., M.S., and Ph.D. degrees from Wuhan University, Wuhan, China, in 2010, 2012, and 2016, respectively.

He is currently an Assistant Professor with the Key Laboratory of Technology in Geo-Spatial Information Processing and Application System, Institute of Electronics, Chinese Academy of Sciences, Beijing, China. His research interests include space, aerial, and close range photogrammetry; computer vision; geometric calibration; bundle adjustment; image rectification, and data quality evaluation.